Kinetic and Mechanistic Studies of the Thermal Decomposition of $Ti(N(CH_3)_2)_4$ during Chemical Vapor Deposition by in Situ Molecular Beam Mass Spectrometry

Edward T. Norton, Jr. and Carmela Amato-Wierda*

Materials Science Program, University of New Hampshire, Durham, New Hampshire 03824

Received May 11, 2001. Revised Manuscript Received September 19, 2001

Various aspects of the kinetics and mechanism occurring during the gas-phase thermal decomposition of $Ti(N(CH_3)_2)_4$, tetrakis(dimethylamido)titanium, have been determined by in situ molecular beam mass spectrometry coupled to a chemical vapor deposition reactor. The rate of $Ti(N(CH_3)_2)_4$ decomposition was measured between 333 and 583 K. The rate constants increase with reactor surface area to volume ratio (S/V), particularly above 530 K ($S/V = 0.118$ mm^{-1}), which indicates a change in mechanism at higher temperatures. For $S/V = 0.118$ mm^{-1}, the Arrhenius parameters between 300 and 530 K are $E_a = 16 \pm 2$ kJ mol^{-1} and $A = 32 \pm 4$ s^{-1}. For the high-temperature regime above 530 K, $E_a = 166 \pm 16$ kJ mol^{-1} and $A = (1.6 \pm 0.2) \times 10^{16}$ s^{-1}. These parameters are consistent with the following mechanistic interpretation for $Ti(N(CH_3)_2)_4$ decomposition: activated adsorption to the walls at low temperatures, followed by gas-phase unimolecular decomposition in combination with some surface process at higher temperatures. Mass spectral evidence supports β-hydride elimination and metallacycle formation as the TDMAT decomposition pathways.

Introduction

Chemical vapor deposition (CVD) is an important synthetic method in which solid materials, typically thin films, are produced from a chemically reactive gas flow. It is the chemical reactions during CVD that distinguish it from physical vapor deposition methods. Knowledge of both gas-phase and surface reactions during CVD is necessary to rationally optimize the film properties, on the basis of a fundamental understanding of the chemistry during the deposition process. Additionally, kinetic and mechanistic data of these chemical reactions are critical for the development of numerical modeling of deposition processes.

In particular, previous results from our group demonstrated that gas-phase chemistry during CVD of titanium silicon nitride (Ti−Si−N) from tetrakis(dimethylamido)titanium (TDMAT or $Ti(N(CH_3)_2)_4$), NH_3, and SiH_4 is critical. Most importantly, it was established that TDMAT activates silane in the presence of ammonia at 723 K.[1] The amount of silane activation is dependent upon the relative amounts of TDMAT and ammonia. Furthermore, the amount of silicon incorporation in the thin films deposited under similar conditions was consistent with the trends observed in the gas-phase experiments. This demonstrated that knowledge of the gas-phase mechanisms that occur during the CVD of Ti−Si−N can be useful as a means of controlling the film composition.

Ti−Si−N is a refractory amorphous ternary nitride which is a promising candidate for future hard coatings in the tool industry[2−4] and diffusion barrier applications in metallization schemes of integrated circuits.[5−9] Currently, titanium nitride (TiN) thin films are extensively used for both of the above applications. TiN has high hardness, excellent chemical resistance, and high electrical conductivity. However, the limits of TiN are being approached in both of these industries. High-speed milling and cutting processes require that tool coatings have improved hardness and oxidation resistance over TiN.[4] In the microelectronics industry, improved diffusion barriers are required for new copper metalization processes and smaller feature sizes.[5,8] The addition of silicon to TiN to form Ti−Si−N addresses both of these problems. Ti−Si−N thin films show increased oxidation resistance and enhanced hardness with increasing Si concentration (up to 200% harder than TiN at ∼10 at % Si).[10,11] Ti−Si−N diffusion barriers show good resistance against copper, and CVD deposition processes

* To whom correspondence should be addressed.

(1) Amato-Wierda, C. C.; Norton, E. T., Jr.; Wierda, D. A. *Chem. Mater.* **1999**, *11*, 2775−2779.
(2) Shin, H.-K.; Shin, H.-J.; Lee, J.-G.; Kang, S.-W.; Ahn, B.-T. *Chem. Mater.* **1997**, *9*, 76−80.
(3) Llauro, G.; Hillel, R.; Sibieude, F. *Chem. Vap. Deposition* **1998**, *4*, 247−252.
(4) Diserens, M.; Patscheider, J.; Levy, F. *Surf. Coat. Technol.* **1998**, *108−109*, 241−246.
(5) Smith, P. M.; Custer J. S. *Appl. Phys. Lett.* **1997**, *70*, 3116−3118.
(6) Reid, J. S. Ph.D. Dissertation, California Institute of Technology, Pasadena, CA, 1995.
(7) Sun, X.; Reid, J. S.; Kolawa, E.; Nicolet, M. A. *J. Appl. Phys.* **1997**, *81*, 656−663.
(8) Sun, X.; Reid, J. S.; Kolawa, E.; Nicolet, M. A. *J. Appl. Phys.* **1997**, *81*, 664−671.
(9) Raaijmakers, I. J. *Thin Solid Films* **1994**, *247*, 85−93.
(10) Vaz, F.; Rebouta, L.; Ramos, S.; da Silva, M. F.; Soares, J. C. *Surf. Coat. Technol.* **1998**, *108−109*, 236−240.
(11) Kim, K. H.; Park, B. H. *Chem. Vap. Deposition* **1999**, *5*, 275−279.

10.1021/cm0104708 CCC: $20.00
Published on Web 11/10/2001

yield the highly conformal films required for future devices.[8]

CVD methods for TiN deposition include a high-temperature process (~1200 K) which typically uses $TiCl_4$ and NH_3 or $TiCl_4$ and N_2/H_2 as precursors, and is used on substrates that are relatively temperature insensitive, such as cutting tools and other refractory materials.[3,5] There is an impetus toward decreasing deposition temperatures, which has led to new precursor systems and processing methods. One low-temperature precursor system for thermal CVD of TiN involves NH_3 and metal−organic compounds such as $Ti(NR_2)_4$ (R = CH_3 or CH_2CH_3), which reduces the deposition temperature to ~725 K. This process has been studied extensively for use in the microelectronics industry.[12−27] Both of these precursor systems have been adapted to deposit Ti−Si−N, with the addition of a silicon source such as silane, disilane, or various chlorosilanes.[3,5,11]

To further unravel the complex chemistry of the ternary precursor system TDMAT/SiH_4/NH_3, it is valuable to understand the thermal decomposition of the individual reactants. Although the thermal decomposition of individual reactants may not be the dominant mechanism for the formation of TiN or TiSiN films, these intramolecular reactions may be important under certain conditions. The work described here focuses on molecular beam mass spectrometry (MBMS) studies of the kinetics and mechanisms of the thermal decomposition of TDMAT alone, without ammonia or silane.

MBMS is a powerful, real-time, in situ technique that samples the gas-phase species of the CVD process to which it is coupled. MBMS is a well-established technique that has been used to analyze the gas-phase chemistry of flames,[28] plasma CVD of diamond, biomass feedstock, and pyrolytic recycling processes.[29−31] MBMS allows direct sampling of the gas phase. The gas which passes through the sampling aperture undergoes a reversible, adiabatic expansion, which rapidly quenches any thermal chemistry. The center of the expansion passes through a second aperture, forming a collisionless beam which travels to the ion source of the mass spectrometer. Thus, species which reach the detector have not undergone any thermal reactions or collisions since being sampled. These features of molecular beam sampling allow it to sample ions, radicals, and neutrals of both condensable and noncondensable species. The technique has the ability to be quantitative. Finally, gases can be sampled from a wide range of experimental conditions, including those of industrial interest.

We have utilized this technique to study the kinetics and mechanisms of the thermal decomposition of TDMAT. The rate constants and Arrhenius parameters for TDMAT decomposition between 333 and 583 K are presented below. Additionally, mass spectral evidence is presented for the proposed mechanisms.

Experimental Section

The experimental apparatus consists of a precursor inlet system and a high-temperature flow reactor which are coupled to a quadrupole mass spectrometer by a four-stage, differentially pumped molecular beam sampling system. The apparatus is shown schematically in Figure 1.

The precursor inlet system is constructed from 6.35 mm outer diameter stainless steel tubing (316L) connected using Swagelok fittings and stainless steel bellows valves. Gaseous precursors are delivered by mass flow controllers (MKS Instruments) which enable accurate and repeatable delivery of known molar quantities. TDMAT liquid (Aldrich, 99.99%) is contained in a 25 mL glass bubbler and delivered by argon carrier gas (Airgas, 99.999%). The TDMAT was used as received and handled in a dry nitrogen glovebox. The carrier gas flow, bubbler pressure, and bubbler temperature determine the precursor flow rate, which are controlled by a mass flow controller, a pressure control valve capacitance manometer feedback system downstream from the bubbler, and a constant-temperature water bath, respectively. The amount of TDMAT delivered to the reactor is calculated using the equation[32]

$$m_{\mathrm{TDMAT}}(\mathrm{sccm}) = m_{\mathrm{carrier}}(\mathrm{sccm})\left(\frac{P_{\mathrm{TDMAT}}}{P_{\mathrm{total}} - P_{\mathrm{TDMAT}}}\right) \quad (1)$$

where m_{TDMAT} is the mass flow rate of TDMAT, m_{carrier} is the mass flow rate of the carrier gas through the bubbler, and P_{total} is the total bubbler pressure. P_{TDMAT} is the vapor pressure of TDMAT calculated from eq 2

$$\log(P_{\mathrm{TDMAT}}(\mathrm{Torr})) = -3.05\left(\frac{1000}{T}\right) + 9.22 \quad (2)$$

where T is the temperature in Kelvin.[33] The temperature in the bubbler is held constant at 342.5 K, at which the vapor pressure of TDMAT is ~2.1 Torr. P_{total} is held at 200 Torr, which fixes the TDMAT flow concentration at 1.04%, or a flow rate of $0.0104 m_{\mathrm{carrier}}$ (sccm).

The precursor/carrier gas mixture was delivered through heated lines (~350 K) to prevent precursor condensation. All gases were delivered to the reactor through a moveable injector, which allows introduction of the precursors at various distances along the reactor tube. Changing the injector position

(12) Sugiyama, K.; Sangryul, P.; Takahashi, Y.; Motojima, S. *J. Electrochem. Soc.* **1975**, *122*, 1545−1549.
(13) Fix, R. M.; Gordon, R. G.; Hoffman, D. M. *Chem. Mater.* **1990**, *2*, 235−241.
(14) Fix, R. M.; Gordon, R. G.; Hoffman, D. M. *Chem. Mater.* **1991,** *3*, 1138−1148.
(15) Musher, J. M.; Gordon, R. G. *J. Mater. Res.* **1996**, *11*, 989−1001.
(16) Musher, J. M.; Gordon, R. G. *J. Electrochem. Soc.* **1996**, *143*, 736−744.
(17) Hoffman, D. M. *Polyhedron* **1994**, *13*, 1169−1179.
(18) Katz, A.; Feingold, A.; Pearton, S. J.; Nakahara, S.; Ellington, M.; Chakrabarti, U. K.; Geva, M.; Lane, E. *J. Appl. Phys.* **1991**, *70*, 3666−3677.
(19) Katz, A.; Feingold, A.; Nakahara, S.; Pearton, S. J.; Lane, E.; Geva, M.; Stevie, F.A.; Jones, K. *J. Appl. Phys.* **1992**, *15*, 993−1000.
(20) Sun, S. C.; Tsai, M. H. *Thin Solid Films* **1994**, *253*, 440−444.
(21) Paranjpe, A.; IslamRaja, M. *J. Vac. Sci. Technol., B* **1995**, *13*, 2105−2114.
(22) Truong, C. M.; Chen, P. J.; Corneille, J. S.; Oh, W. S.; Goodman, D. W. *J. Phys. Chem.* **1995**, *99*, 8831−8842.
(23) Dubois, L. H.; Zegarski, B. R.; Girolami, G. S. *J. Electrochem. Soc.* **1992**, *139*, 3603−3609.
(24) Prybyla, J. A.; Chiang, C.-M.; Dubois, L. H. *J. Electrochem. Soc.* **1993**, *140*, 2695−2702.
(25) Dubois, L. H. *Polyhedron* **1994**, *13*, 1329−1336.
(26) Weiler, B. H. *Chem. Mater.* **1995**, *7*, 1609−1611.
(27) Weiler, B. H. *J. Am. Chem. Soc.* **1996**, *118*, 4975−4983.
(28) Biordi, J. C. *Prog. Energy Combust. Sci.* **1977**, *3*, 151−173.
(29) Rego, C. A.; May, P. W.; Henderson, C. R.; Ashford, M. N. R. In situ mass spectrometric study of the gas-phase species involved in CVD of diamond as a function of filament temperature. *Proceedings of the 5th European Conference on Diamond and Related Materials*, Tuscany, Italy, Sept 25−30, 1994.
(30) Hsu, W. L.; Tung, D. M. *Rev. Sci. Instrum.* **1992**, *63*, 4138−4148.
(31) Nimlos, M. R.; Milne, T. A. *Environ. Sci. Technol.* **1992**, *26*, 545−552.
(32) Hersee, S. D.; Ballingall, J. M. *J. Vac. Sci. Technol., A* **1990**, *8*, 800−804.
(33) Intemann, A.; Koerner, H.; Koch, F. *J. Electrochem. Soc.* **1993**, *140*, 3215−3222.

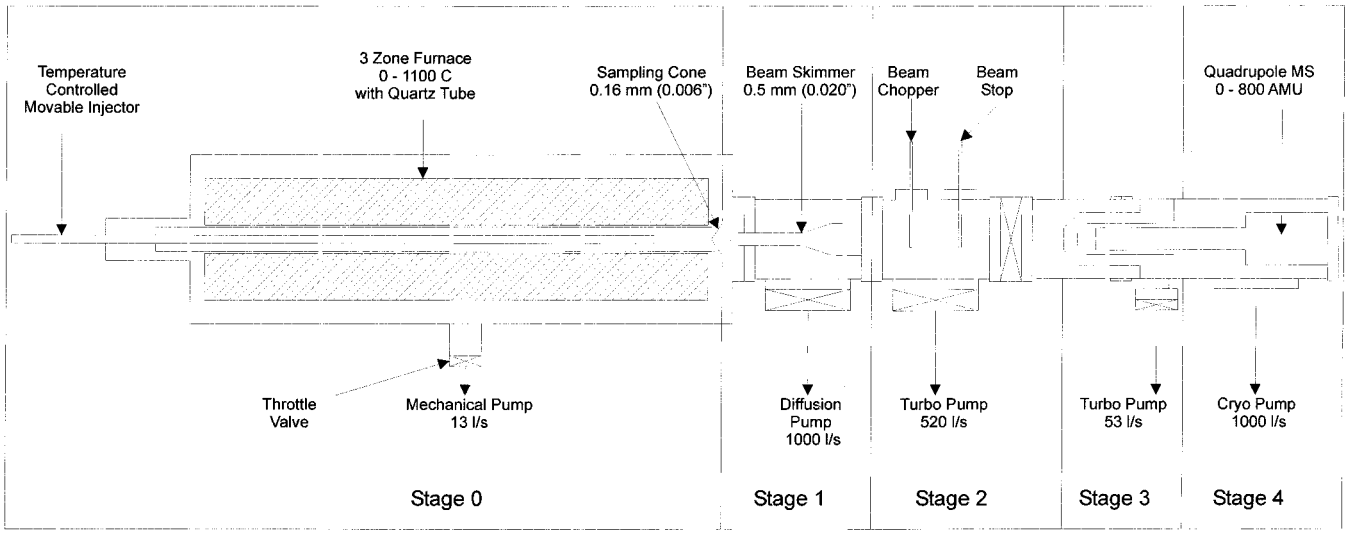

Figure 1. Schematic of the molecular beam mass spectrometer coupled to the CVD reactor.

and gas flow velocity in the reactor enables the residence time (reaction time) to be changed. The injector is water-jacketed and held 10 K higher than the bubbler temperature; this is high enough to avoid precursor condensation, yet cool enough to prevent excessive preheating of the precursor prior to its introduction into the reactor.

The flow reactor is a quartz tube which is 61 cm long and has an inner diameter of 3.8 cm. It is resistively heated in three zones, and is capable of reaching 1370 K. The temperature is measured by type K thermocouples located at six evenly spaced intervals along the length of the reactor. Constant temperature in the reactor is maintained by an electronic temperature controller (PID type) and a solid-state relay which controls the power being delivered to the heating elements. The temperature controllers were calibrated using a shielded thermocouple in the center of the gas flow.

An aperture at the exit of the reactor samples the gas flow at the centerline of the reactor tube during CVD and forms it into a molecular beam, which is then skimmed and collimated before entering the ion source of a quadrupole mass spectrometer (Merlin system, ABB Extrel). The mass spectrometer (*m*/*e* 0−800) has an electron impact ionizer (50 eV), an energy analyzer, and a continuous dynode electron multiplier with a conversion dynode. Measurements of the TDMAT signal intensity are normalized to argon, which is used as an internal standard to account for variations in instrument sensitivity.

Measurements of the rate constants for TDMAT decomposition were taken between 333 and 583 K (60−310 °C). The total reactor pressure was maintained at 2.70 ± 0.05 Torr by means of a capacitance manometer throttle valve control loop. The surface area to volume ratio (*S*/*V*) was varied by packing the reactor with quartz inserts. Rate constants were determined by monitoring the TDMAT molecular ion signal (*m*/*e* 224) at several reaction times at each temperature, taking a 3 min signal average at each. The residence time (reaction time) in the reactor was varied by changing the gas flow velocity, while the injector to molecular beam sampling aperture distance was held constant.

The total reactor pressure was varied to determine the pressure dependence of TDMAT decomposition. The TDMAT decomposition rate was determined at six different reactor pressures from 0.95 to 51.60 Torr. This was done at 548 K (275 °C), with the reactor at low *S*/*V* (no quartz inserts).

Mass spectra were collected from *m*/*e* 5 to *m*/*e* 235 (*m*/*e* 1 step size, 1 s dwell time), during the decomposition of TDMAT at 2.7 Torr. Data were collected at six temperatures: 343, 393, 453, 503, 543, and 553 K. Data were also collected at four different reaction times, corresponding to 40%, 50%, 60%, and 70% decomposition of the TDMAT parent molecule.

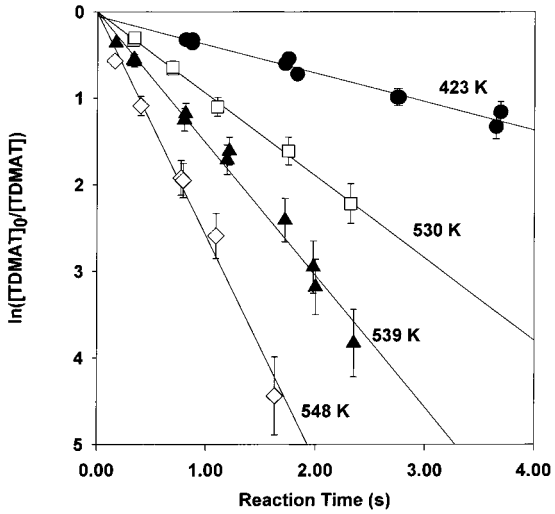

Figure 2. Natural log of the normalized TDMAT signal decay versus reaction time at four representative temperatures.

Results

Figure 2 is a semilog plot of the TDMAT (mol wt 224) signal normalized to the initial concentration versus reaction time, at four representative temperatures. The error bars shown are for 1 standard deviation. TDMAT decay exhibits first-order kinetics throughout this temperature range. The slopes of the first-order decay plots provide the rate constants for the TDMAT thermal decomposition.

To determine the contribution from surface reactions to the TDMAT decay, the rate constants were measured at two surface area to volume ratios: $S/V(\text{low}) = 0.118$ mm^{-1} and $S/V(\text{high}) = 0.708$ mm^{-1}. The effect of this *S*/*V* ratio on the rate constant of the TDMAT decay is shown in Figure 3 as a function of temperature. Below 480 K, increasing the *S*/*V* ratio only increases the rate constants ~10%. Above 480 K, increasing the *S*/*V* ratio substantially increases the rate constants by more than 15-fold.

The Arrhenius plot of the natural log of the rate constant versus inverse temperature is shown in Figure 4 for both *S*/*V* ratios. The slopes and intercepts provide values of the TDMAT decomposition activation energy

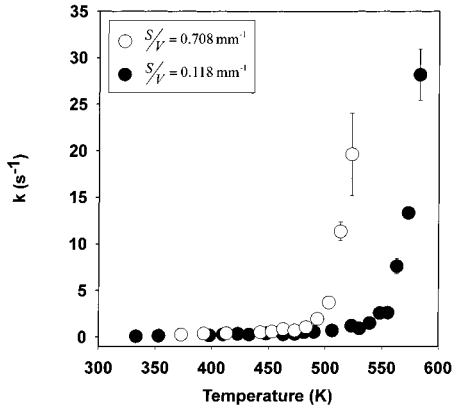

Figure 3. Effect of the *S*/*V* ratio on the rate constant of TDMAT decay.

(E_a) and preexponential factor (A), respectively. The plot exhibits two temperature regimes distinguished by different slopes and intercepts, indicating a change in the TDMAT decomposition mechanism. This change in mechanism occurs at 530 K for low *S*/*V* and at 480 K for high *S*/*V*. At low *S*/*V*, the Arrhenius parameters are $E_a = 16 \pm 2$ kJ mol^{-1} and $A = 32 \pm 4$ s^{-1} for the low-temperature regime and $E_a = 166 \pm 16$ kJ mol^{-1} and $A = (1.6 \pm 0.2) \times 10^{16}$ s^{-1} for the high-temperature regime. At high *S*/*V*, the calculated activation energies are statistically identical to the low *S*/*V* values, and the preexponential values are 35 ± 8 and $(4.2 \pm 0.6) \times 10^{17}$ s^{-1} for the low- and high-temperature regimes, respectively. These values are summarized in Table 1.

Figure 5 shows a log−log plot of the experimental rate constants for TDMAT decomposition versus total reactor pressure (Torr), at 548 K. The error bars shown are for 2 standard deviations. This temperature was chosen to be above the transition temperature seen in Figure 4 for low *S*/*V*. The horizontal line is the expected pressure dependence for a TDMAT molecule over the pressure range shown. The line of best fit seemingly suggests that the rate increases as pressure decreases, but due to the large variation in the data, this is not statistically different from the expected pressure dependence, at a 95% confidence level. This is evident since the confidence intervals for the lines of best fit (dashed lines) contain the values of the expected pressure dependence.

Table 1. Summary of the Calculated Arrhenius Parameters for TDMAT Decomposition[a]

high temperature	E_a (kJ mol^{-1})	A ($\times 10^{16}$ s^{-1})
low *S*/*V*	166 ± 16	1.6 ± 0.2
high *S*/*V*	163 ± 24	42 ± 6.0
low temperature	**E_a (kJ mol^{-1})**	**A (s^{-1})**
low *S*/*V*	16 ± 2	32 ± 4
high *S*/*V*	15 ± 3	35 ± 8

[a] High-temperature data are calculated using rate constants above 530 K (low *S*/*V*) and 480 K (high *S*/*V*), and low-temperature data are calculated using rate constants below these temperatures.

Shown in Figure 6 is a typical mass spectrum of the gas phase sampled during TDMAT decomposition at 503 K, and a residence time of 750 ms. The species labeled on the spectrum are products of the postulated mechanisms for gas-phase decomposition of TDMAT from previously published computational studies.[34] The schemes for the proposed mechanisms are shown in Figure 7. The peaks present in the spectrum are from (1) undecomposed TDMAT, (2) reaction intermediates, (3) decomposition products, and (4) fragments of all the above generated in the mass spectrometer ion source. Unfortunately, peaks from fragments of undecomposed TDMAT overlap with many of the peaks from decomposition products and their fragments. This makes it difficult to conclusively determine whether the detected species were formed in the reactor or in the ionizer. To accurately establish whether a species was from decomposition or ionization, baseline mass spectra were collected at conditions with negligible amounts of TDMAT decomposition (<10% decomposition at 343 K and 500

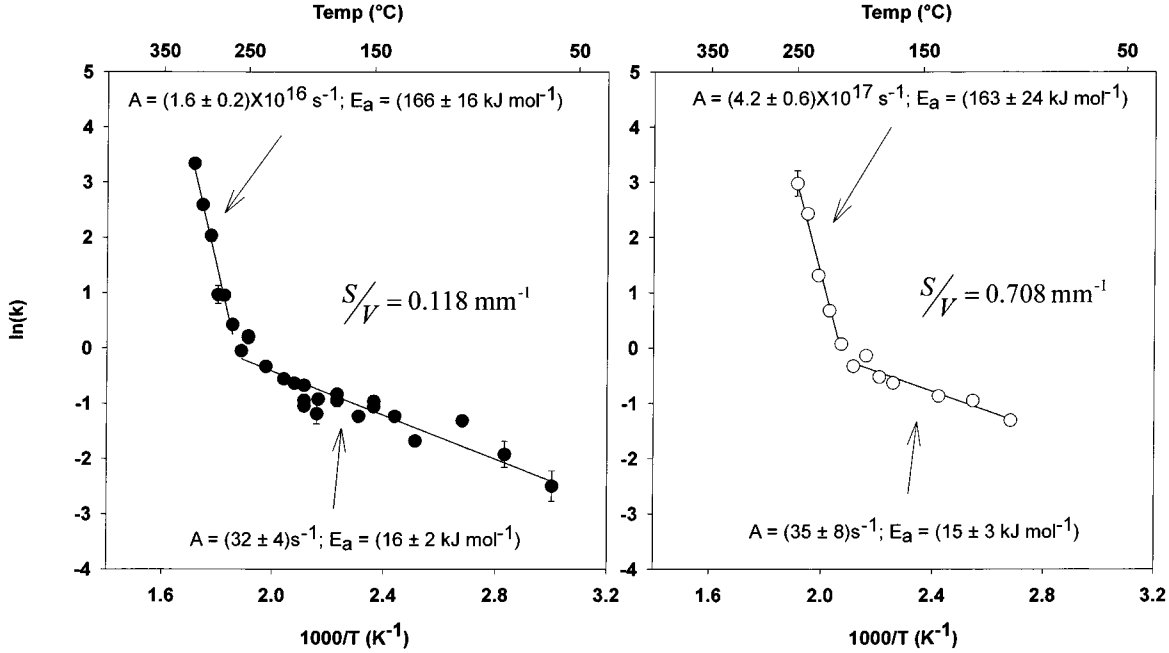

Figure 4. Arrhenius plot for TDMAT decomposition for both surface area to volume ratios. Dark lines represent a weighted linear least-squares fit to the data, each of which is labeled with the corresponding Arrhenius parameters.

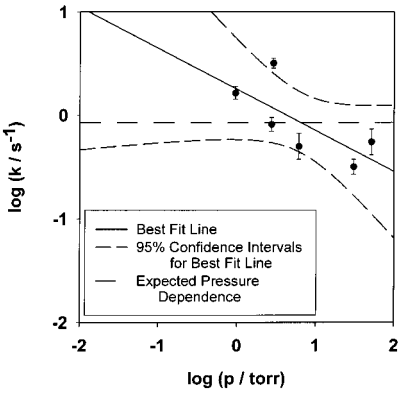

Figure 5. Log−log plot of TDMAT decomposition rate vs reactor pressure at 548 K. The horizontal line represents the theoretical pressure dependence for TDMAT assuming a unimolecular decomposition mechanism. The solid line represents the line of best fit for the data, shown with 95% confidence intervals.

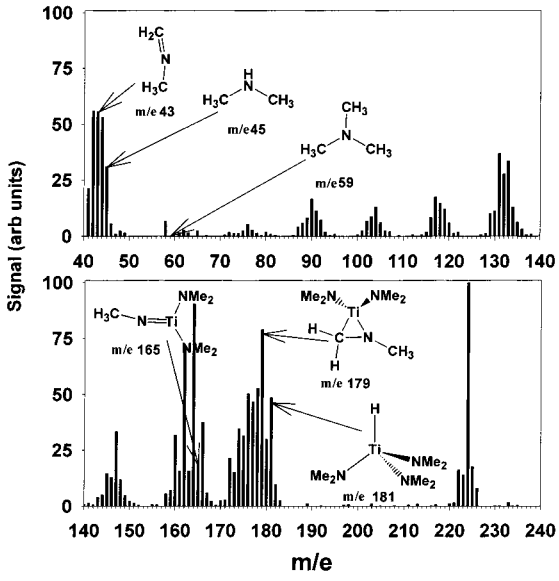

Figure 6. Mass spectrum of TDMAT decomposition at 503 K and 750 ms reaction time. Product species from the proposed mechanism[34] are shown where they would appear.

ms). The baseline spectra show the TDMAT ion fragmentation pattern, and were subtracted from the decomposition spectra collected at other conditions.

Discussion

Kinetics of TDMAT Thermal Decomposition. The low activation energies and small preexponential factors calculated for the low-temperature regimes of the Arrhenius plots are consistent with an activated adsorption surface process.[35] In other words, TDMAT decay is largely a result of adsorption to the reactor walls at low temperature. Numerous molecules have an activation energy for surface adsorption, followed by dissociation.[36] Adsorption processes typically have preexponential factors between 10^2 and 10^4 s^{-1}, which is within an order of magnitude of the experimentally determined values,[36]

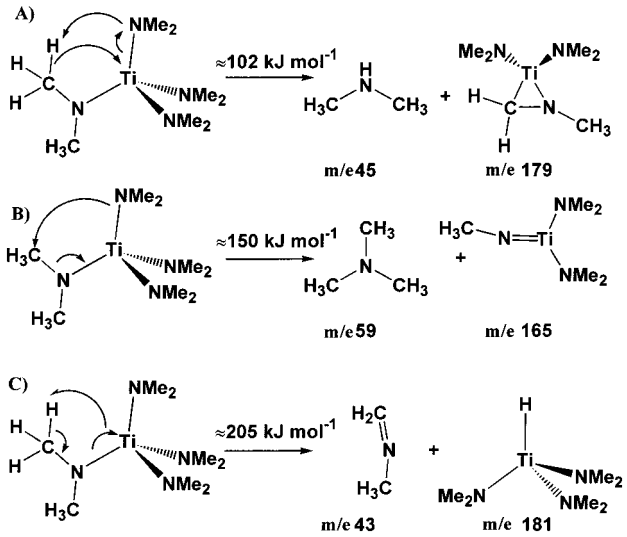

Figure 7. Proposed mechanisms for gas-phase decomposition as applied to TDMAT. Beneath each product species is shown the location of its molecular ion peak, if it were to appear. Above each reaction arrow is shown an estimated activation energy as calculated for the TDMAT analogue used by Cundari and Morse.[34]

32−35 s^{-1}. Additionally, the relatively low activation energy of 16 kJ mol^{-1} is typical for physisorption of molecules on surfaces.[35]

For the high-temperature regime in the Arrhenius plot, the preexponential factors and activation energies support the existence of a gas-phase mechanism, in addition to the surface process revealed by the enhanced rate constant at the higher *S*/*V* ratio. Gas-phase fission of complex precursor molecules into two fragments typically[37] results in *A* values between 10^{15} and 10^{17} s^{-1}. The 166 kJ mol^{-1} activation energy is also within the range of computational values reported in the literature for the decomposition of a model analogue of TDMAT, namely, $TiH_2(NH_2)(N(H)CH_3)$.[32]

Temperature-programmed desorption (TPD) studies in the literature of pure surface reactions of TDMAT on TiN surfaces support the above observations.[22] It was found that most of the TDMAT adsorbed on a TiN surface desorbs as the intact precursor by 350 K. This is in agreement with our Arrhenius parameters, which are consistent with adsorption to the reactor walls. Decomposition of the remaining adsorbed TDMAT begins at approximately 510 K, which is near the temperature at which a significant surface process becomes evident in the data in Figure 4. The studies of TDMAT on TiN substrates were chosen for comparison to the experiments reported here, because the walls of the reactor most closely represent a TiN-coated surface due to decomposed TDMAT.

Recently, Jensen et al. studied the decomposition of TDMAT on surfaces in the temperature range of 473−623 K, at 5 Torr.[38] It was found that below 478 K the reaction rate was very slow, with no observed gas-phase reactions, and that above 478 K TDMAT decomposition increased drastically as other reactions competed with the slow surface reaction, resulting in fewer gaseous

(34) Cundari, T. R.; Morse, J. M. *Chem. Mater.* **1996**, *8*, 189−196.
(35) Hudson, J. B. *Surface Science: An Introduction*; Butterworth-Heinemann: Woburn, MA, 1992.
(36) Somorjai, G. A. *Chemistry in Two Dimensions: Surfaces*; Cornell University Press: Ithaca, NY, 1981.
(37) Holbrook, K. A.; Pilling, M. J.; Robertson, S. H. *Unimolecular Reactions*, 2nd ed.; John Wiley & Sons: New York, 1996.
(38) Driessen, J. P. A. M.; Schoonman, J.; Jensen, K. F. *J. Electrochem. Soc.* **2001**, *148*, G178−G184.

species observed. The measured reaction rates in Figure 4 are similarly slow below 480 K, and our Arrhenius parameters for this regime are consistent with surface reaction processes. Our high-temperature data also support a change in surface mechanism, revealed by the rate enhancement due to higher surface area to volume ratios.

Pressure Dependence of TDMAT Thermal Decomposition. Unimolecular decomposition reactions are energized by collisions with thermalized buffer gas, in accordance with the Lindemann−Hinshelwood mechanism.[37,39−41] This theory predicts that the parent molecule becomes excited by collision processes, and exists in equilibrium with unexcited parent molecules. A fraction of the activated molecules then decompose into reaction products. The decomposition process clearly follows first-order kinetics; however, the activation process is a second-order process. At pressures below a critical pressure (falloff pressure), the reaction rate decreases as pressure decreases. Above the falloff pressure, the overall reaction appears as pseudo-first-order and is constant.[37,39−41] The falloff pressure is directly related to the number of internal degrees of freedom a molecule possesses. For a molecule such as TDMAT ($N = 37$), the falloff pressure is expected to be approximately 10^{-3} Torr, above which the rate constant should not change.[37]

As seen in Figure 5, the line for the expected pressure dependence falls within the confidence interval for the line of best fit. This shows that there is no significant pressure dependence for TDMAT decomposition from 0.95 to 51.60 Torr.

Mechanistic Study of TDMAT Thermal Decomposition. A theoretical study of small-molecule elimination from a TDMAT analogue, $TiH_2(NH_2)(N(H)CH_3)$, performed by Cundari and Morse[34] has shown that several postulated mechanistic pathways exist for its decomposition. These mechanisms are shown in Figure 7 for TDMAT. Pathway 1 involves the transfer of a proton to a dimethylamido group, which leaves as dimethylamine. This leaves a metallacycle Ti−C−N ring that can undergo successive reactions. The second pathway, a 1,2-elimination, involves the transfer of an intact methyl group to a dimethylamido group, resulting in trimethylamine, and a titanium imido species with a double bond between the Ti metal center and nitrogen. The third reaction pathway involves the transfer of a proton to the metal center, resulting in the β-hydride product and methylmethyleneamine. The proposed mechanisms are listed in increasing order of activation energy as calculated for the analogue molecule.

The metallacycle formation reaction would initially produce dimethylamine and the Ti−C−N metallacycle; peaks that could correspond to those species are present in the mass spectrum. Previous researchers have postulated the existence of the metallacycle product on the basis of evidence from FTIR[23] gas-phase studies and XPS[42] surface experiments. Also seen are peaks at *m*/*e* 43 and 181 that would correspond to the products from the β-hydride elimination. Noticeably absent are peaks corresponding to both products of the 1,2-elimination reaction. Titanium-containing species have a very pronounced isotope pattern (as seen around the TDMAT parent ion at *m*/*e* 224), and this accounts for the small peak found at *m*/*e* 165.

The experimentally determined activation energy for the gas-phase decomposition reaction (164 kJ mol^{-1}, average) is of the same order of magnitude as all of the computed activation energies (102, 150, and 205 kJ mol^{-1}). However, the mass spectral evidence supports the β-hydride and metallacycle formation mechanisms. Therefore, it is most likely that these two mechanisms, as well as surface adsorption, are operative during the thermal CVD involving TDMAT.

Conclusions

As part of a larger effort to understand the complex chemistry of the TDMAT + SiH_4 + NH_3 CVD process, the gas-phase kinetics of the TDMAT thermal decomposition were measured between 333 and 583 K. The rate constants for TDMAT decomposition increased when the reactor *S*/*V* ratio was increased 6-fold, indicating the contribution of a surface process; this is particularly manifest at temperatures above 480 K. The Arrhenius plot of the rate constants versus inverse temperature exhibits a change in slope and intercept at approximately 500 K, consistent with a change in the mechanism responsible for TDMAT decomposition. For the case of the lower *S*/*V* ratio, the low-temperature (<530 K) Arrhenius parameters are $E_a = 16 \pm 2$ kJ mol^{-1} and $A = 32 \pm 4$ s^{-1}. The low preexponential factor and activation energy are appropriate for an activated adsorption process. For the high-temperature regime above 530 K, $E_a = 166 \pm 16$ kJ mol^{-1} and $A = (1.6 \pm 0.2) \times 10^{16}$ s^{-1}. These Arrhenius parameters are consistent with a gas-phase unimolecular decomposition of a complex molecule. However, the change in *S*/*V* revealed a surface component at all temperatures, with the greatest contribution above 480 K. Therefore, above this temperature, TDMAT decay results from a combination of gas-phase and surface processes. Mass spectral evidence supports that the β-hydride elimination and metallacycle formation mechanisms are the dominant pathways in the gas-phase decomposition of TDMAT.

Acknowledgment. We gratefully acknowledge financial support provided by the National Science Foundation (Grant DMR-9631794 and Career Award DMR-9875062) and the University of New Hampshire.

CM0104708

(39) Moore, J. W.; Pearson, R. G. *Kinetics and Mechanism*, 3rd ed.; John Wiley & Sons: New York, 1981; pp 219−222.

(40) Laidler, K. J. *Chemical Kinetics*, 3rd ed.; Harper & Row: New York, 1987; 150−157.

(41) Steinfeld, J. I.; Francisco, J. S.; Hase, W. L. *Chemical Kinetics and Dynamics*; Prentice Hall: Upper Saddle River, NJ, 1989.

(42) Ruhl, G.; Rehmet, R.; Kni_ová, M.; Merica, R.; Vep_ek, S. *Chem. Mater.* **1996**, *8*, 2712−2720.